Spectral Analysis of Radiation-Induced Natural Convection in Littoral Waters

Yadan Mao, Chengwang Lei, John C. Patterson

Abstract—The mixing of pollutions and sediments in near shore regions of natural water bodies depends heavily on the characteristics such as the strength and frequency of flow instability. In the present paper, the instability of natural convection induced by absorption of solar radiation in littoral regions is considered. Spectral analysis is conducted on the quasi-steady state flow to reveal the power and frequency modes of the instability at various positions. Results indicate that the power of instability, the number of frequency modes, the prominence of higher frequency modes, and the highest frequency mode increase with the offshore distance and/or Rayleigh number. Harmonic modes are present at relatively low Rayleigh numbers. For a given offshore distance, the position with the strongest power of instability is located adjacent to the sloping bottom while the frequency modes are the same over the local depth. As the Rayleigh number increases, the unstable region extends toward the shore.

Keywords—Instability, Littoral waters, natural convection, Spectral analysis

I. INTRODUCTION

TERRESTRIALLY derived solutes and particulates in lakes, reservoirs and other geophysical water bodies pose a significant challenge to human health. The resilience of the littoral water to pollutions depends largely on the natural processes that contribute to the transport and dilution of the pollution, such as wind driven currents and waves. For regions under relatively calm conditions, natural convection in littoral regions plays an important role in the transport of nutrients and pollutants across these water bodies.

As the depth of water increases in the offshore direction in the near shore region, during the daytime, the approximately equal amount of heating is distributed over a varying depth of water; therefore, the water at a given location is either hotter or cooler than its horizontal neighbouring region, driving an exchange flow offshore near the surface and on shore at depth. Similarly, night cooling drives a flow in the opposite direction.

Y. Mao is with the School of Engineering, James Cook University, Townsville, QLD 4811, Australia (+61-7-47815234; fax: +61-7-47816788; e-mail: yadan.mao@jcu.edu.au).

C. Lei is with the School of Engineering, James Cook University, Townsville, QLD 4811, Australia (e-mail: chengwang.Lei@jcu.edu.au).

J. C. Patterson is with the School of Engineering, James Cook University, Townsville, QLD 4811, Australia (e-mail: john.patterson@jcu.edu.au).

The significance of natural convection in littoral region has been confirmed in field observations [1-3]. It is found that natural convection induced by the near shore geometry acts as a "thermal siphon", which substantially reduces the time required to replace the water in the littoral region.

In order to facilitate understanding and simplify the problem, a simple model has been proposed by Farrow and Patterson for natural convection in near shore waters [4-5]: In this model, it is assumed that an approximately equal amount of heating or cooling is uniformly distributed over the varying depth of water as the offshore distance varies, resulting in a horizontal temperature gradient that drives the flow. However, upon a closer examination, the simple model is not physically realistic in that it assumes a uniform distribution of heat over the local water depth. In fact, during the daytime, the water body absorbs solar radiation in an exponentially decaying manner with water depth. For a closer representation of realistic situations, another model [6-8] takes the fact of decaying radiation into consideration, and assumes that any radiation energy reaching the sloping bottom is absorbed by the bottom and reemitted as a bottom heat flux. The bottom heat flux induces an adverse temperature gradient near the sloping bottom, which is a potential source of instability in the form of thermal plumes rising up from the bottom, enhancing vertical mixing. This vertical mixing has significant implications to the distribution of suspended particulates along the local water depth. In order to reveal the power and frequency of this vertical mixing, the present paper focuses on the spectral analysis of the time series of flow properties for the unstable flow, which will reveal the variation of spectra with offshore distance, local water depth and Rayleigh number. Previously, efforts to understand the characteristics of this radiation-induced stability have been made through both linear stability analysis [9] and direct three dimensional stability analyses [10]. The former derived the critical Grashof number for instability as a function of the horizontal position, while the latter examined the stability properties of flow in the initial and transitional stages, which reveals the variation of the onset time of instability, the transverse wave number and the growth rate of instability with offshore distance. In comparison to [10], which is concerned with the stability properties in the initial and transitional stage, the present paper will focus on the later stage of the flow development — the quasi-steady stage, during which the spectra of the flow is steady with respect to time [8].

A prerequisite for the present research is ascertaining the extent of unstable flow region. Extending the scaling analysis of [7], the scaling analysis of [8] includes a scaling for the

World Academy of Science, Engineering and Technology
International Journal of Physical and Mathematical Sciences
Vol:3, No:5, 2009

extent of the unstable region, which has been verified by numerical simulations.

II. MODEL FORMULATION

The daytime circulation in the near shore waters is modelled with a wedge with a bottom slope of A and a water depth of h (Fig.1). With Boussinesq assumption, the Navier-Stokes and energy equations governing the flow and temperature evolution within the wedge can be written as:

$$\frac{\partial u}{\partial x} + \frac{\partial v}{\partial y} = 0 , \qquad (1)$$

$$\frac{\partial u}{\partial t} + u\frac{\partial u}{\partial x} + v\frac{\partial u}{\partial y} = -\frac{1}{\rho_0}\frac{\partial p}{\partial x} + v\nabla^2 u , \qquad (2)$$

$$\frac{\partial v}{\partial t} + u\frac{\partial v}{\partial x} + v\frac{\partial v}{\partial y} = -\frac{1}{\rho_0}\frac{\partial p}{\partial y} + v\nabla^2 v + g\beta(T - T_0) , \qquad (3)$$

$$\frac{\partial T}{\partial t} + u\frac{\partial T}{\partial x} + v\frac{\partial T}{\partial y} = k\nabla^2 T + S(x,y,t) , \qquad (4)$$
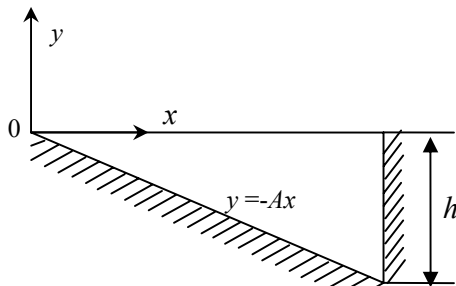

Fig. 1 Geometry of the flow domain

where u and v are the velocity components in the horizontal and vertical directions, x and y are the horizontal and vertical coordinates originating from the tip; T is the fluid temperature; and p is the pressure. The density, kinematic viscosity, thermal diffusivity and thermal expansion coefficient of the water at the reference temperature T_0 are denoted by ρ_0, v, k and β respectively. $S(x,y,t)$ in Equation (4) represents the internal heating source due to absorption of solar radiation. The radiation intensity at a particular wavelength decreases with the water depth according to Beer's law:

$$I = I_0 e^{\eta y} \qquad y \le 0 , \qquad (5)$$

where I_0 is the radiation intensity at the water surface, η is the attenuation coefficient of water which is a function of the wave-length of the incident radiation and the turbidity of water [11]. The attenuation coefficient is often assumed to be constant in applications to simplify the problem, and this assumption is also adopted here. Therefore, the source term in equation (4) is given by:

$$S = H_0 \eta e^{\eta y} \qquad -Ax \le y \le 0 , \qquad (6)$$

where $H_0 = I_0/(\rho_0 C_p)$, and C_p is the specific heat of water at the reference temperature.

In the present model, a rigid non-slip boundary condition is assumed for the bottom slope ($u = v = 0$) and the deep-end wall, and the water surface is assumed to be stress free

($\partial u/\partial y = 0$ and $v = 0$). An adiabatic temperature condition is assumed for the water surface and the end wall. It is assumed that the bottom slope absorbs the radiation energy reaching the slope and reemits it in a form of a bottom heat flux:

$$\frac{\partial T}{\partial \hat{n}} = -\frac{1}{k}H_0 e^{-A\eta x} , \qquad (7)$$

where $\hat{n}$ is the unit vector normal to the slope. The temperature of the water body increases through both direct absorption of radiation and the bottom heat flux. The former forcing results in a stable stratification of water body and thus no flow is generated through this mechanism. In contrast, a thermal boundary layer adjacent to the bottom slope is generated through the latter mechanism, and within this boundary layer, a horizontal temperature gradient drives the water up the slope. The adverse temperature gradient near the bottom slope is a potential source for thermal instability.

In order to investigate the characteristic of instability, it is essential to ascertain the criteria for instability to occur and the extent of instability. These issues are addressed in the scaling analysis of [8]. It is revealed that for the unstable flow regime, as offshore distance increases, the dominant mode of heat transfer changes from conduction into stable convection, and finally into unstable convection. Some of the scaling results reported in [8] that are directly relevant to the present research are summarized below.

The criteria for instability to occur at offshore distance x is

$$Ra > f_2(x), \qquad (8)$$

where Ra is the global Rayleigh number defined as

$$Ra = \frac{g\beta H_0 h^4}{v k^2} , \qquad (9)$$

and $f_2(x)$ is the local critical Rayleigh number function for instability to happen, which is derived as

$$f_2(x) \sim Ra_c^3 (h/x)^4 e^{A\eta x} , \qquad (10)$$

where Ra_c is the critical Rayleigh number of an inclined thermal layer which can be approximated by [12]:

$$Ra_c = Ra_c(0^\circ)/\cos\theta , \qquad (11)$$

where θ is the inclination angle of the thermal layer, and $Ra_c(0^\circ)$ is the critical Rayleigh number for horizontal fluid layers, which is constant.

For the shallow water where $h < 4/\eta$, $f_2(x)$ decreases monotonically in the offshore direction. From (8) and (10), it follows that instability occurs if

$$Ra > f_2(x)_{min} \sim Ra_c^3 A^4 e^{\eta h} , \qquad (12)$$

The function $f_2(x)$ becomes infinite as $x \to 0$, indicating that there is always a stable region near shore. The position x_0 that divides the unstable region offshore from the stable region near shore is determined from

$$f_2(x_0) \sim Ra . \qquad (13)$$

Given the complex nature of the $f_2(x)$ function (refer to (10)), no explicit form of x_0 can be obtained from (13). However, x_0 can be easily determined numerically from (13).

With the guidance of the above scaling results, the following sections will focus on the characteristics of instability through spectral analysis on the time series of flow properties obtained from numerical simulations.

World Academy of Science, Engineering and Technology
International Journal of Physical and Mathematical Sciences
Vol:3, No:5, 2009

III. NUMERICAL PROCEDURES

With radiation being constantly applied and no heat loss from the boundaries, the average temperature of the water body keeps increasing. The average temperature T_0 can be derived through the balance between the energy entering into the water body and the energy absorbed by the water body.

$$T_0 = \frac{2H_0}{h}t . \tag{14}$$

After subtracting the average temperature T_0 from the local temperature T, a quasi-steady state for the residual temperature T_1 can be reached [7]. The thermal boundary conditions for T also apply to T_1 since only temperature gradients are involved in these conditions. A new set of equations with T_1 can be derived with the following non-dimensional form:

$$\frac{\partial u}{\partial x} + \frac{\partial v}{\partial y} = 0 , \tag{15}$$

$$\frac{\partial u}{\partial t} + u\frac{\partial u}{\partial x} + v\frac{\partial u}{\partial y} = -Pr\,Ra\frac{\partial p}{\partial x} + Pr\nabla^2 u , \tag{16}$$

$$\frac{\partial v}{\partial t} + u\frac{\partial v}{\partial x} + v\frac{\partial v}{\partial y} = -Pr\,Ra\frac{\partial p}{\partial x} + Pr\nabla^2 v + Pr\,RaT_1, \tag{17}$$

$$\frac{\partial T_1}{\partial t} + u\frac{\partial T_1}{\partial x} + v\frac{\partial T_1}{\partial y} = \nabla^2 T_1 + (\eta e^{\eta y} - 2) , \tag{18}$$

where Pr is the Prandtl number defined as

$$Pr = \nu/k . \tag{19}$$

All the quantities are non-dimensional after normalizing the governing equations with the following scales: the length scale $x, y \sim h$; the time scale; $t \sim h^2/k$; the temperature scale $T_1 \sim H_0 h / k$; the velocity scale: $u,v \sim k/h$; and the pressure gradient scale: $p_x, p_y \sim \rho_0 g H_0 h / k$.

The governing equations (15)-(18) along with the specified boundary and initial conditions are solved numerically using a finite volume method. The SIMPLE scheme is adopted for pressure-velocity coupling; and the QUICK scheme is applied for spatial derivatives. A second-order implicit scheme is applied for time discretization in calculating the transient flow.

The simulation is conducted in a triangular domain of a dimensionless depth of $h = 1$ and a bottom slope of $A = 0.1$, with a non-dimensional attenuation coefficient $\eta = 0.12$ and a Prandtl number $Pr = 7$. In order to avoid a singularity at the tip, the tip is cut off at $x = 0.2$, and an extra non-slip and adiabatic vertical wall is assumed there. The cut region accounts for only 0.04% of the full domain, and thus no significant modification to the flow is anticipated.

For the spectral analysis of the numerical results, a horizontal convection rate averaged over the local depth, which characterizes the strength of heat transfer, is calculated from the numerical results as:

$$H(x) = \frac{1}{Ax}\int_{-Ax}^{0} uT_1 dy . \tag{20}$$

where $H(x)$ is normalized by I_0.

IV. RESULTS AND DISCUSSIONS

As described in [8], based on the time series of flow properties, the development of the flow can be classified into three stages: initial, transitional, and quasi-steady. For the unstable flow regime, the initial stage is characterized by rapid increasing of the magnitude of flow properties. As instability sets in, the transitional stage begins, which is characterized by fluctuations with large amplitude variations. Finally, the flow reaches the quasi-steady state with regular and steady fluctuations, and the spectrum of flow properties becomes steady during the quasi-steady state. As mentioned previously, the spectrum of the quasi-steady state is the focus of the present paper, and therefore the quasi-steady state of each time series is identified for the spectral analysis.

From the scale (12), it follows that for the current parametric settings, the Rayleigh number need to be larger than $\sim 1.5\times 10^5$ in order for instability to occur. In this study, we consider Rayleigh numbers in the range of 1.4×10^6 to 1.4×10^7. A mesh and time step dependency test has been conducted for $Ra = 1.4\times 10^7$ with three different meshes, 211×71, 315×105 and 421×141. Since the spectra at different positions are the focus of this paper, the influence of mesh resolution on the spectrum of the vertical component of velocity at $x = 4.0$, $y = -0.3$ is examined. The time steps for different meshes are adjusted accordingly so that the CFL (Courant-Freidrich-Lewy) number remains approximately the same for all the meshes. Fig. 2 shows the spectra of the vertical velocity over a dimensionless time period of 0.1 at the quasi-steady state obtained with different meshes. The spectrum variation among different meshes suggests that the spectrum is sensitive to the density of the mesh, which is in fact one of the features of the transition from laminar to turbulent flow. Higher frequencies are more prominent in denser grids. However, the numerical results presented in Table 1 suggest that the numerically predicted values of major stability properties are converging as the mesh density increases. Furthermore, the Rayleigh number tested here is the highest among all the calculated cases; the effect of the grid resolution on the solution is expected to be less significant for other cases with lower Ra. In order to ensure the accuracy of the solutions, the grid 421×141 is used in all the following simulations. For the chosen mesh, the minimum face area is 0.0024; the maximum is 0.5125; and the maximum stretch factor is 1.07. The time step adopted for this mesh is 2.0×10^{-5}, giving a maximum CFL number of 1.02 for the present Rayleigh number.
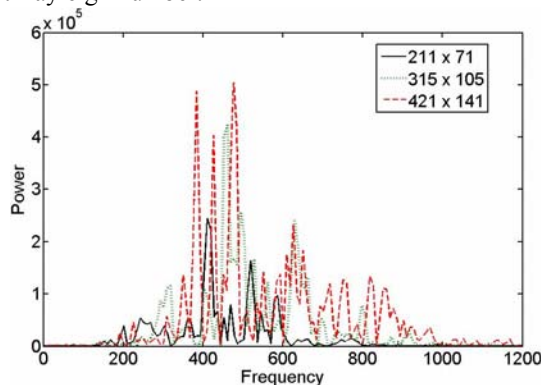

Fig. 2 Spectra of the time series of the vertical component of velocity at $x = 4.0$, $y = -0.3$ for $Ra = 1.4\times 10^7$ from different meshes

World Academy of Science, Engineering and Technology
International Journal of Physical and Mathematical Sciences
Vol:3, No:5, 2009

TABLE I
PROPERTIES OF THE VERTICAL COMPONENT OF VELOCITY AT $x = 4.0$, $y = -0.3$
FOR DIFFERENT GRIDS

	1. 211×71	2. 315×105	3. 421×141	Variation 1&2	Variation 2&3
f_d	410.8	461.1	475.7	11.5%	3.1%
P_d	$2.5×10^5$	$4.2×10^5$	$5.0×10^5$	50.8%	17.4%
std	52.3	58.8	60.7	11.7%	3.2%
mean	23.6	22.9	22.5	3.0%	1.8%

Note: 'f_d' denotes the most dominant frequency, 'P_d' denotes the power of the most dominant frequency. "std" denotes the standard deviation of the time series at quasi-steady sate. "mean" demotes the vertical component of velocity averaged over the time series during quasi-steady state.

A. Spectral Variation with Water Depth

At a given offshore distance, spectral variation with water depth is investigated based on the time series of temperature at different local water depths for $Ra = 3.5 ×10^6$ as shown in Fig. 3. It is clear that for a certain offshore distance, the frequency modes at different water depths are the same, with the strongest power locating near the bottom slope. As the adverse temperature gradient near the bottom slope triggers instability, thermal plumes originate near the bottom slope. As the plumes travel upwards, their power is diminished by the stable stratification in the upper part induced by the direct absorption of radiation. A comparison between Figs 3 (a) and (b) suggests that as offshore distance increases, the higher frequency modes become more pronounced. Spectral analysis on flow velocities suggests the same trend of spectral variation as revealed by temperature.
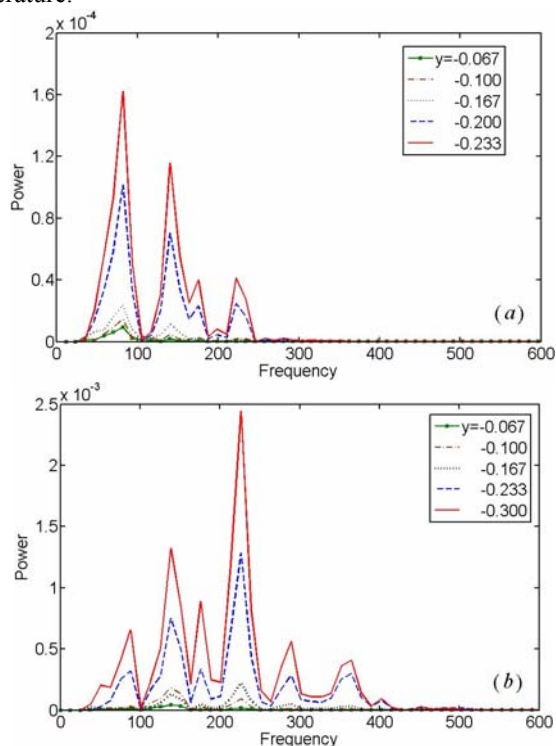

Fig. 3 Spectra of temperatures at different depths over the vertical line of (a) $x = 2.67$ and (b) $x = 3.33$ for $Ra = 3.5×10^6$

B. Spectra Variation with Offshore Distance

The above section suggests that for a given offshore distance, the frequency modes are the same at different water depths. Therefore, the frequency modes revealed by spectral analysis on flow properties integrated along the local water depths, such as $H(x)$ defined in (20), applies to local positions along the vertical line.

To investigate the variation of stability properties with the horizontal position, the quasi-steady-state time series of $H(x)$ is plotted in Fig 4 for $Ra = 2.1×10^6$ at $x = 3.33$ and 4.17. Comparison suggests that the amplitude of the fluctuations increases with the offshore distance. In order to further illustrate the characteristics of instability, spectral analysis was conducted to reveal the variation of the power and the frequencies with offshore distance and Rayleigh number. Fig. 5 shows the results based on $H(x)$ obtained at two different horizontal positions $x = 3.33$ and 4.17 for $Ra = 1.4×10^6$, $2.1×10^6$ and $3.5×10^6$ respectively.
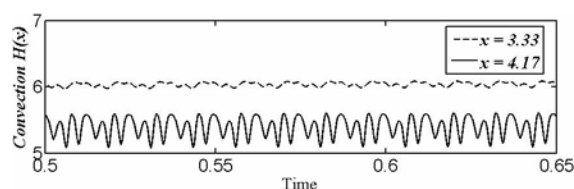

Fig. 4 The quasi-steady-state time series of $H(x)$ at $x = 3.33$ and 4.17 for $Ra = 2.1×10^6$
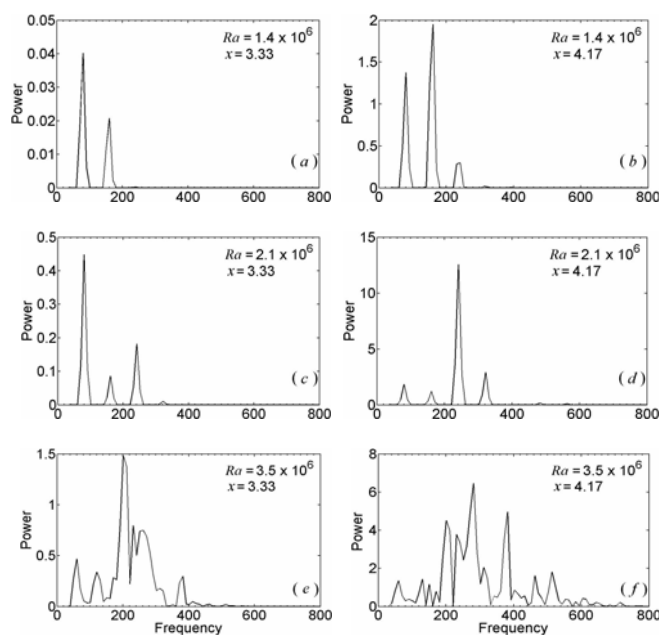

Fig. 5 The spectra of time series of horizontal convection $H(x)$ at the quasi-steady state for different Rayleigh numbers at two horizontal positions

It is clear in Fig. 5 that for a certain Ra, higher frequency modes become more prominent as the offshore distance and/or Rayleigh number increases. For $Ra = 1.4×10^6$ and $2.1×10^6$, the spectra are of distinct harmonic modes with the lowest frequency mode of $f = 80.5$. As the Rayleigh number continues

World Academy of Science, Engineering and Technology
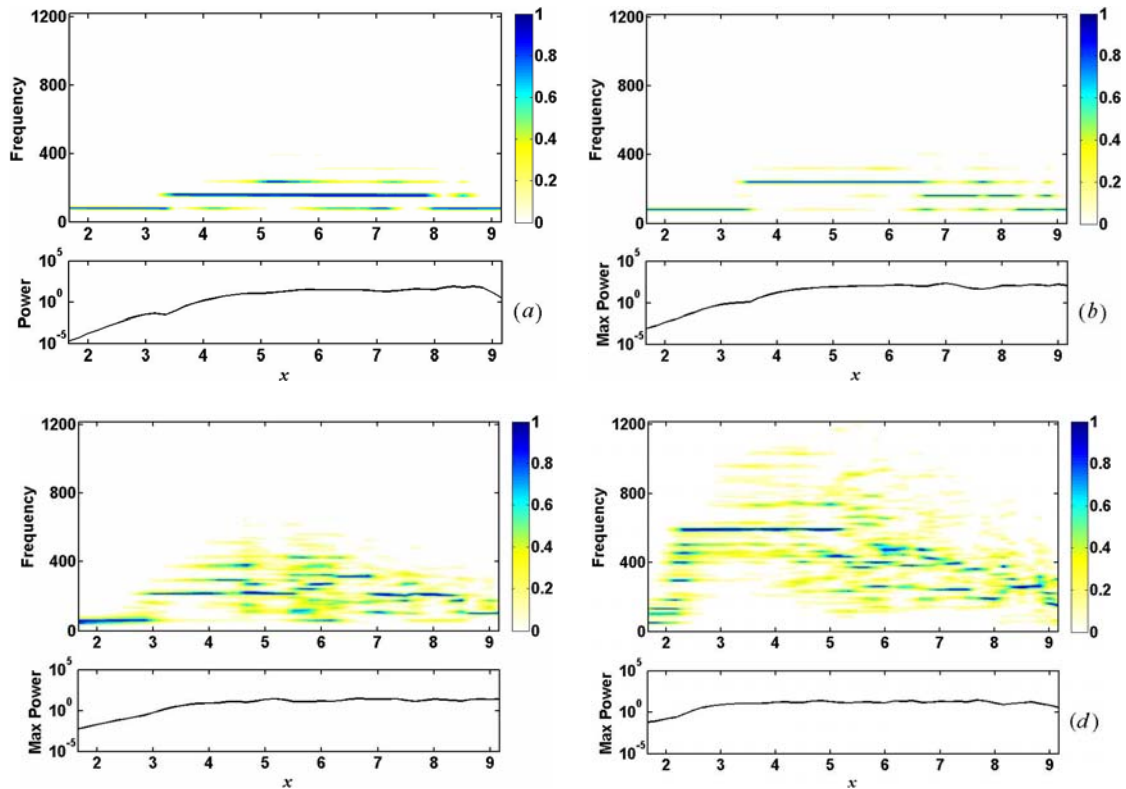International Journal of Physical and Mathematical Sciences
Vol:3, No:5, 2009

Fig. 6 Spectra of average horizontal convection $H(x)$ normalized by the maximum power of each x position for different Rayleigh numbers. (a) $Ra = 1.4 \times 10^6$ (b) $Ra = 2.1 \times 10^6$ (c) $Ra = 3.5 \times 10^6$ (d) $Ra = 1.4 \times 10^7$

to increase, for $Ra = 3.5 \times 10^6$, the interaction between different frequency modes becomes stronger, as a result, the frequency bands become connected with each other, and thus the harmonic mode disappears. The above variation of the spectra with Ra suggests that for the unstable flow regime, there is a transition from harmonic frequency modes to non-harmonic modes as Ra increases.

The above results reveal the spectra variation at discrete offshore distances. In order to further illustrate the spectra variation over a wide range of offshore distances, the spectra at various offshore distances need to be plotted together for comparison. Since the magnitude of the maximum spectral power varies significantly with offshore distance, as shown in Fig. 5, the spectra at various offshore distances are normalized by the maximum power of the respective spectrum. In this way, the spectral power varies from 0 to 1 at any offshore distance and a frequency mode map showing the spectral variation with offshore distance is generated. This is shown in Fig. 6. For reference, the maximum power as a function of offshore position is plotted beneath each of the spectral plots.

The variation of frequency mode and power with offshore distance and Rayleigh number is clearly illustrated in Fig. 6. It is worth mentioning that the region near the end-wall is strongly affected by the end-wall which forces a return flow [8], and in turn significantly influences the stability property of the flow near the end-wall region. Therefore the frequency modes in the region affected by the end wall are expected to be different from the unaffected-region, which is confirmed in Fig. 6. For the unaffected region, the prominence of higher

frequency modes increases with offshore distance for a given Rayleigh number. As a result, the dominant frequency mode shifts from low frequency to higher frequency as offshore distance increases. In contrast, this trend can not be observed in the region near the end wall, where the frequency modes become complicated and irregular because of the end wall effect. As the Rayleigh number increases, for a given offshore distance, both the number of frequency modes and the prominence of higher dominant frequency modes increase. Meanwhile, for the near shore region where the maximum power is small, the maximum power for a certain offshore distance increases with the Rayleigh number, indicating the extension of unstable region toward the shore as the Rayleigh number increases, which is similar to the trend suggested by the standard deviation of $H(x)$ reported in [8].

V. Conclusion

As the critical function of instability was derived as a function of offshore distance, the extent of instability for a given Rayleigh number can be predicted by the previous scaling analysis of [8]. Following the previous investigation, the properties of instability in the near shore water induced by absorption of radiation are investigated in the present paper through the spectral analysis. While the direct stability analysis of [10] has investigated the stability properties at the initial and transitional stage, the present paper is focused on the stability properties at the quasi-steady state, when the spectra of the flow become steady. It is worth noting that the investigations of both

World Academy of Science, Engineering and Technology
International Journal of Physical and Mathematical Sciences
Vol:3, No:5, 2009

[10] and the present paper focus on the shallow water case, in which the depth of water is less than the penetration depth of radiation, and therefore, the bottom heat flux resulting from the absorption of residual radiation is dominant.

It is revealed that for a given offshore distance, the frequency modes are the same over the local depth, and the position with the strongest power of fluctuation locates adjacent to the sloping bottom, indicating the vertical position of strongest mixing dynamism.

For a certain Rayleigh number, the power of fluctuation and the prominence of higher frequency mode increase in the offshore direction. As a result, the dominant frequency shifts from low frequency modes to high frequency modes as offshore distance increases. Therefore, the dynamism of mixing induced by absorption of radiation increases in the offshore direction. Harmonic modes are present at relatively low Rayleigh numbers, and as the Rayleigh number increases, the interaction between different modes becomes stronger and thus frequency bands become connected with each other and the harmonic modes disappear. In addition, the number of frequency modes and the highest dominant frequency increase with the Rayleigh number.

The thermal instability induced by absorption of radiation discussed here is only part of the many natural processes that triggers instability in near shore waters. Thermal instability may also triggered by night time cooling and other processes as long as the adverse temperature gradient is over a certain critical value. The effect of thermal instability may at times be swamped by instability induced by other mechanisms such as wind and waves. An incorporation of thermal instability into the model of near-shore processes will result in a more comprehensive model.

REFERENCES

[1] E. E. Adams and S. A. Wells, "Field measurements on side arms of Lake," *Journal of hydraulic Engineering*, vol. 110, pp. 773–793, 1984.
[2] S. G. Monismith, J. Imberger and M. L. Morison, "Convective motions in the sidearm of a small reservoir," *Limnology & Oceanography*, vol. 35, pp. 1676-1702, 1990.
[3] S. G. Monismith, A. Genin, M. A. Reidenbach, G. Yahel and J. R. Koseff, "Thermally driven exchanges between a coral reef and the adjoining ocean," *J. Phys. Oceanogr.*, vol. 36, pp. 1332-1347, 2006.
[4] D. E. Farrow and J. C. Patterson, "On the response of a reservoir sidearm to diurnal heating and cooling," *J. Fluid Mech.*, vol. 246, pp. 143-161, 1993a.
[5] D. E. Farrow, "Periodically forced natural convection over slowly varying topography," *J. Fluid Mech.*, vol. 508, pp. 1-21, 2004.
[6] D. E. Farrow & J. C. Patterson, "The daytime circulation and temperature structure in a reservoir sidearm," *Int. J. Heat Mass Transfer*, vol. 37, pp. 1957-1968, 1994.
[7] C. Lei and J. C. Patterson, "Unsteady natural convection in a triangular enclosure induced by absorption of radiation," *J. Fluid Mech.*, vol. 460, pp. 161-184, 2002.
[8] Y. Mao, C. Lei and J. C. Patterson, "Unsteady natural convection in a triangular enclosure induced by absorption – A revisit by improved scaling analysis," *J. Fluid Mech.*, accepted, 2008.
[9] D. E. Farrow and J. C. Patterson, "On the stability of near shore waters of a lake when subject to solar heating," *Int. J. Heat Mass Transfer*, vol. 36, pp. 89-100, 1993b.
[10] C. Lei and J. C. Patterson, "A direct stability analysis of a radiation-induced natural convection boundary layer in a shallow wedge," *J. Fluid Mech.*, vol. 480, pp. 161-184, 2003.
[11] A. Rabl and C. E. Nielsen, "Solar ponds for space heating," *Solar Energy*, vol. 17, pp.1-12, 1975.
[12] U. H. Kurzweg, "Stability of natural convection within an inclined channel," Trans. ASME C: J. Heat Transfer, vol. 92, pp. 190-191, 1970.